Research Square

Preprints are preliminary reports that have not undergone peer review.
They should not be considered conclusive, used to inform clinical practice,
or referenced by the media as validated information.

Milling characteristics of SiCp/2024Al composites thin-walled part based on movable auxiliary support

Gao Zhijie
Zhu Peng
Yang Shu
Wei Zuoshan
Wang Qitong
zhou li (lizhou@ytu.edu.cn)
Yantai University

Research Article

Keywords: SiCp/Al composite, Milling processing, Auxiliary support, Finite element simulation, Residual stress

Posted Date: June 8th, 2023

DOI: https://doi.org/10.21203/rs.3.rs-3013727/v1

License: This work is licensed under a Creative Commons Attribution 4.0 International License.
Read Full License

Milling characteristics of SiCp/2024Al composites thin-walled part based on movable auxiliary support

Zhijie Gao[1] · Peng Zhu[1] · Shu Yang[1] · Zuoshan Wei[2] · Qitong Wang[2] · Li Zhou[1]

Abstract Due to milling force and milling heat, thin-walled parts are highly susceptible to deformation and even scrap. In this paper, a method of milling thin-walled part based on the movable auxiliary support was proposed, and the second developed VDLOAD subroutine was used to simulate the movement of auxiliary support. The influences of the magnitude and area of the movable auxiliary support on the surface temperature, deformation and residual stress of the workpiece were investigated. The results showed that, with the increasing of the magnitude and area of the movable auxiliary support, both surface temperature and deformation of the workpiece decrease. The tensile residual stress decreases and gradually changes to compressive residual stress. Interestingly, when the magnitude of the movable auxiliary support exceeds 20 MPa or the area exceeds 100 mm^2, the deformation of the workpiece continues to decrease, but the middle of the workpiece is concave towards the milling cutter. It is worth noting that the effect of movable auxiliary support area on the residual stress does not show a clear regularity. Thus, the reasonable auxiliary support can reduce deformation and stability in the milling of thin-walled parts and the results of the study can provide a theoretical basis for optimizing the milling process of thin-walled parts.

Keywords SiCp/Al composite · Milling processing · Auxiliary support · Finite element simulation · Residual stress

1. Introduction

SiCp/Al composite possesses excellent physical and mechanical properties, such as low density and thermal expansion coefficient, high specific stiffness, superior corrosion resistance, and therefore is widely used in aerospace and military fields. Recently, SiCp/Al composite thin-walled parts are becoming increasingly common in high-tech applications such as precision optics and electronic packaging [1-3]. However, SiCp/Al composite is a typical difficult-to-machine material with high hardness, brittleness and good wear resistance, which is susceptible to deformation during machining, resulting in low machining accuracy and unstable surface quality [4]. Especially, during milling of thin-walled parts, it is difficult to control the machining

✉Li Zhou
Lizhou@ytu.edu.cn

✉Zuoshan Wei
15376251006@163.com

[1] School of Electromechanical and Automotive Engineering, Yantai University, Yantai 264005, China

[2] Shandong Key Laboratory of Advanced Aluminium Materials and Technology, Binzhou Institute of Binzhou, Binzhou 256606, China

accuracy because of its weak stiffness and easy deformation under the action of milling force and residual stress [5,6].

To ensure machining accuracy, deformation control is required during the milling process. Zhang et al. [7] proposed an active control method to reduce the deformation of thin-walled part by adjusting the fixture, and avoid the redistribution of residual stress. Wang et al. [8] found that deformation could be effectively reduced and the accuracy could be improved through the reasonable selection of clamping scheme and tool path during milling of Al6061 thin-walled part. Scippa et al. [9] considered the influences of fixturing, tool tip dynamics and material removal to reduce deflections of Aluminum 6082-T4 alloy thin-walled part by optimizing cutting speed. Chen et al. [10] used a finite element method (FEM) to analyse the influence of tool inclination on the elastic deformation of stainless steel 1Cr11Ni2W2MoV thin-walled part, and the results showed that both the milling force and the workpiece deformation were the smallest when the tool inclination was 4 ° or 15 ° . Zhang et al. [11] used the ABAQUS thermo-mechanical coupling analysis module to simulate the milling of SiCp/Al composites thin-walled part, and the results indicated that the deformation of the thin-walled part increased with increasing feed per tooth and cutting width. Jia et al. [12] proposed a method for predicting the deflection of micro-milling thin-walled parts, and verified the accuracy of the results by experiments. Fan et al. [13] analyzed the effects of stress, temperature, cutting force, strain gradient and their dimensions on the cutting deformation during machining SiCp/Al composites from the perspective of material microplasticity mechanics and material dislocation theory.

Residual stress has a significant effect on the service life of parts, including the effects on fatigue strength and corrosion resistance. The milling process causes mechanical and thermal stress on the material, leading to the formation of residual stress on the surface of the workpiece. Therefore, the study of residual stress in milling operations is crucial [14]. Zhang et al. [15] developed a two-dimensional orthogonal cutting finite element model by ABAQUS/Explicit, they found that SiCp/Al composite was machined with surface defects, and the surface residual stress changed from compressive stress to tensile stress. Cui et al. [16] simulated the milling process of SiCp/Al composite and investigated the effects of tool angle, milling depth and milling speed on milling force, temperature, stress and chip. Wu et al. [17] carried out simulation analysis and experimental verification of residual stress on the milled surface of Ti-10V-2Fe-3Al, and proposed a machining process with high feed, high cutting speed and small cutting depth. Kong et al. [18] investigated the effect of milling parameters on the residual stress in Al2024 curved thin-walled part, and the results showed that, within a reasonable range, increasing the milling speed and tool radius can reduce the residual stress. Wang et al. [19] used the finite element analysis software MSC. Marc to simulate the effect of material removal on machining deformation of aluminium alloy pre-stretched plates and found that the release and redistribution of residual stress were the main cause of machining deformation in thin-walled part. Wu et al. [20] conducted finite element simulations and experiments on 7075 aluminium alloy aerospace part using single-sided machining methods and quasi-symmetric machining methods to investigate the mechanism of milling deformation caused by

residual stress, and the result showed the quasi-symmetric machining method could reduce the deformation caused by residual stress.

Most of the current researches on machining of SiCp/Al composites thin-walled part have focused on the effects of milling parameters such as milling speed, feed per tooth and milling depth on deformation and residual stress. In this paper, we proposed a method for milling thin-walled parts based on the movable auxiliary support, which is developed by using Fortran language for secondary development of the ABAQUS software. The influences of moving load magnitude and area on the surface temperature, deformation and residual stress of the workpiece were investigated.

2. FEM simulation

2.1 Modeling processing

First, the VDLOAD user subroutine is developed, which can be used to define the variation of the distributed load magnitude and area as a function of position, time, velocity, etc. For a set of points, each of which appears in an element-based or surface-based of a nonuniform load definition. In the subroutine, the simulation of the movable auxiliary support is written in Fortran language. Then a thermo-mechanical coupling finite element model is used to simulate the regulations of deformation and residual stress in the milling of SiCp/2024Al composites thin-walled part under varying auxiliary support conditions. The overall flow of the finite element simulation is shown in Fig. 1.

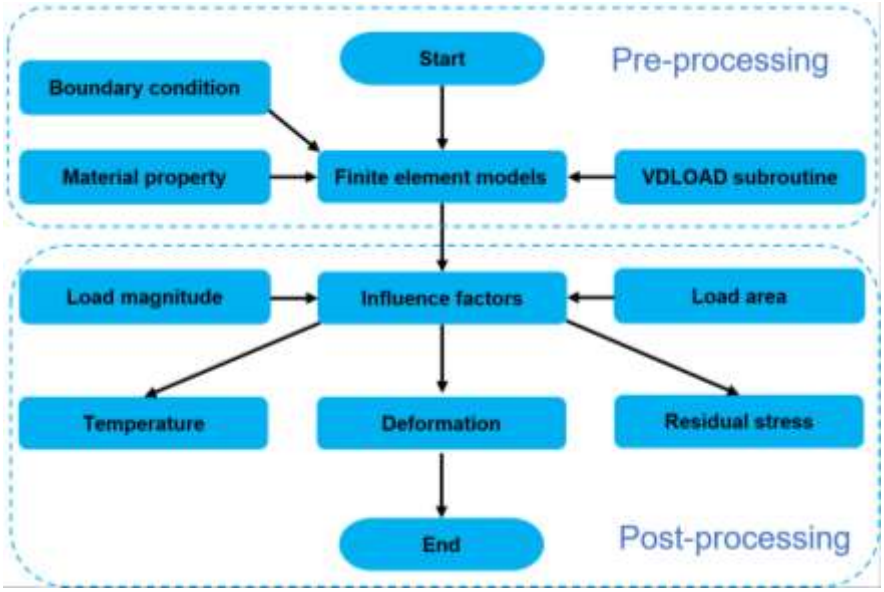

Fig. 1 Milling flow chart of SiCp/2024Al composites thin-walled part

The milling tool model and the thin-walled part model are built by ABAQUS, and the overall milling cutter is a high hardness PCD four-edge end mill. In order to improve the calculation efficiency and study the deformation characteristics of the workpiece, the milling cutter is set as a rigid body without deformation in the simulation analysis. This paper adopts a single factor analysis, and the specific conditions of milling simulation are listed in Table 1.

Table 1 Milling parameters of 45 vol% SiCp/2024Al composite

Spindle speed(r/min)	Milling depth(mm)	Feed per tooth(mm/z)	Rake angle(°)	Relief angle(°)
3600	8	1.5	10	8

Fig. 2a and b show the front and back of the milled workpiece, respectively. In addition, due to the small machining area, transition mesh is used to ensure efficient and accurate, and the "4 to 2" transition method is used, as shown in the local amplified view of Fig. 2a. The schematic diagram of the movable auxiliary support is shown in Fig. 2.

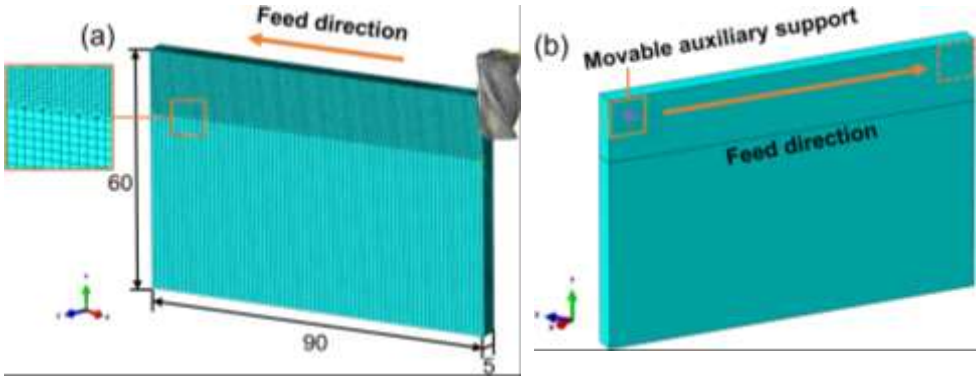

Fig. 2 Schematic diagram of milling SiCp/Al composites thin-walled part :(a) finite element model and transition mesh, (b) movable auxiliary support.

2.2 Material constitutive equation

The milling process involves high strain rates, and large temperature gradients. The relationship between stress, temperature and strain rate can be established in the case of high strain rate in order to accurately describe the deformation characteristics. In this paper, the workpiece material is 45 vol% SiCp/2024Al composite, which is assumed to be isotropic homogeneous. The Johnson–Cook constitutive equation is implemented to model the flow behavior of SiCp/Al composite, which takes into account the influences of thermal softening, strain and strain rate. The equation can be expressed as [21]:

$$\sigma = \left(A + B\varepsilon^{\mathrm{n}}\right)\left(1 + C\ln\frac{\dot{\varepsilon}}{\dot{\varepsilon}_0}\right)\left[1 - \left(\frac{T - T_{\mathrm{r}}}{T_{\mathrm{m}} - T_{\mathrm{r}}}\right)^{\mathrm{m}}\right] \tag{1}$$

where σ is the flow stress, A is the yield stress at the reference temperature and strain rate, B is the strain hardening coefficient, n is the strain hardening exponent, ε^n is the plastic strain, C is the strain rate sensitivity coefficient, $\dot{\varepsilon}$ is the strain rate, $\dot{\varepsilon}_0$ is the reference plastic strain rate, T is the workpiece temperature, T_m and T_r are the material melting and room temperature coefficient, respectively. The relevant exponents are defined as shown below:

Table 2 Material constants of Johnson–Cook model of 45 vol% SiCp/2024Al composite [22]

A(MPa)	B(MPa)	C	m	n	T_m (°C)	T_0 (°C)

300	470.6	0.00952	3.954	0.2558	635	20

Table 3 Material properties of 45 vol% SiCp/2024Al composite [22]

Material properties	SiCp/Al
Young ' s modulus(MPa)	158000
Poisson ' s ratio	0.21
Density(kg/m^3)	2.9x10^3
Thermal conductivity(W/m/°C)	189
Coefficient of thermal expansion(°C^{-1})	1.4 x10^{-5}
Specific heat (J/kg/°C)	850

2.3 Fracture model

For milling simulation, whether the chip separation criterion is reasonable or not is the key factor to ensure the correct milling process. Similarly, the Johnson-Cook damage criterion is used to define chip separation, when the damage parameter D = 1, the material starts to fail. The specific expression is [23]:

$$D = \sum \frac{\Delta \varepsilon^{\mathrm{p}}}{\varepsilon^{\mathrm{f}}} \tag{2}$$

$$\varepsilon^{\mathrm{f}} = \left[d_1 + d_2 \exp\left(-d_3 \eta\right)\right]\left[1 + d_4 \ln\left(\frac{\varepsilon^{p}}{\varepsilon_0}\right)\right]\left[1 + d_5\left(\frac{T - T_{transition}}{T_{melt} - T_{transition}}\right)\right] \tag{3}$$

where $\Delta\varepsilon^{p}$ is the change in equivalent plastic strain, ε_f is the fracture strain, $d_1 - d_5$ is the failure parameters, $\eta = -\frac{p}{q}$ is the stress triaxiality, p is the compressive stress, q is the von Mises equivalent stress, ε_p is the plastic strain rate, $T_{transition}$ is the transition temperature, it does not undergo any deformation at this temperature or below the change temperature. The failure parameters of the material are listed in Table 4.

Table 4 Johnson–Cook damage parameters of 45 vol% SiCp/2024Al composite [22]

d_1	d_2	d_3	d_4	d_5
0.09212	0.3647	-2312	0.04424	0.26

3. Results and discussion

3.1 Temperature field analysis

3.1.1 Effect of movable auxiliary support magnitude

Milling heat is mainly caused by the plastic deformation of the workpiece in the primary shear zone and the tool-chip contact zone, as well as by the friction generated between the tool, chip and workpiece. Milling heat has a great influence on the

machining accuracy and surface quality [24].

Fig.3 shows the surface temperature distributions after milling. It is worth nothing that the highest temperatures about 300 °C during machining are in the contact area between the tool and the workpiece and on the flying chips. It is clear from Fig. 3 that the temperature distribution follows the same pattern at different magnitudes, with the highest temperatures at the end of the thin-walled part and then gradually decreasing towards the start, with a slight tendency to increase at the start. As the magnitude of the movable auxiliary support increases, the high temperature region on the machined surface decreases.

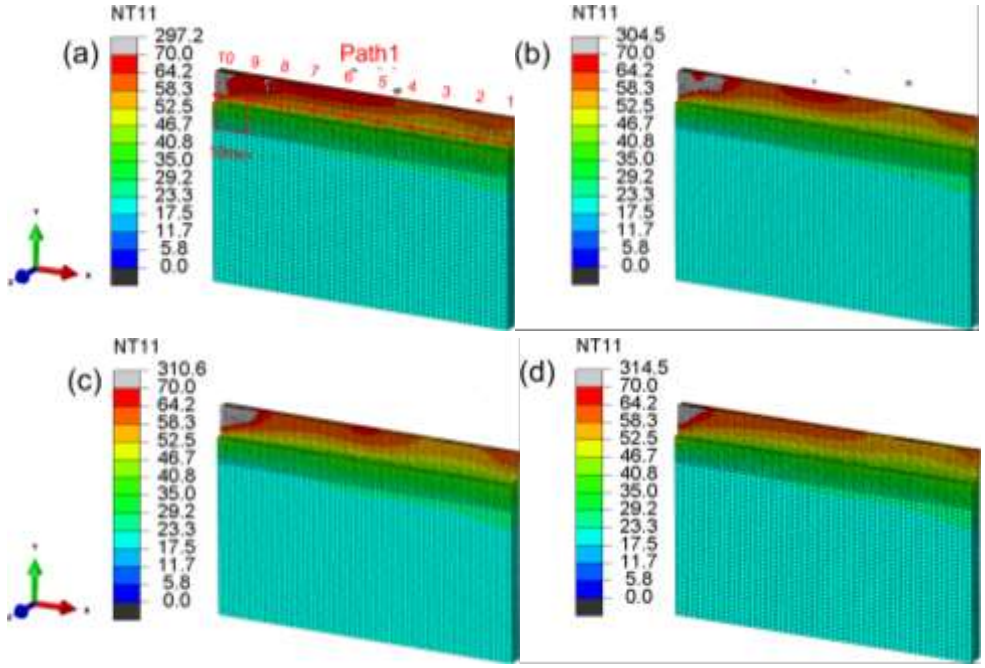

Fig. 3 Temperature distributions for movable auxiliary support magnitudes of (a) 0 MPa, (b) 10 MPa, (c) 20 MPa, (d) 30 MPa.

In order to obtain the effect of movable auxiliary support magnitude on the temperature, 10 points were extracted along the machined surface, each 10 mm apart, as shown in Fig. 3a. Fig. 4 depicts the curve of the surface temperature of the workpiece with the movable auxiliary support magnitude for an auxiliary support area of 100 mm^2. The maximum temperatures for movable auxiliary support magnitudes of 0 MPa, 10 MPa, 20 MPa and 30 MPa are 64.7 °C, 63.4 °C, 59.4 °C and 57.9 °C, respectively. It can be seen the machined surface temperature decreases as the magnitude of the movable auxiliary support increases. The surface temperature is highest at a movable auxiliary support of 0 MPa and lowest at 30 MPa. The reason for this phenomenon is that increasing the movable auxiliary support magnitude causes the thin-walled part to be squeezed, reducing the angle between the milling cutter and the workpiece and facilitating the flow of chips. High chips evacuation then removes a large amount of heat, reducing the temperature of the machined surface.

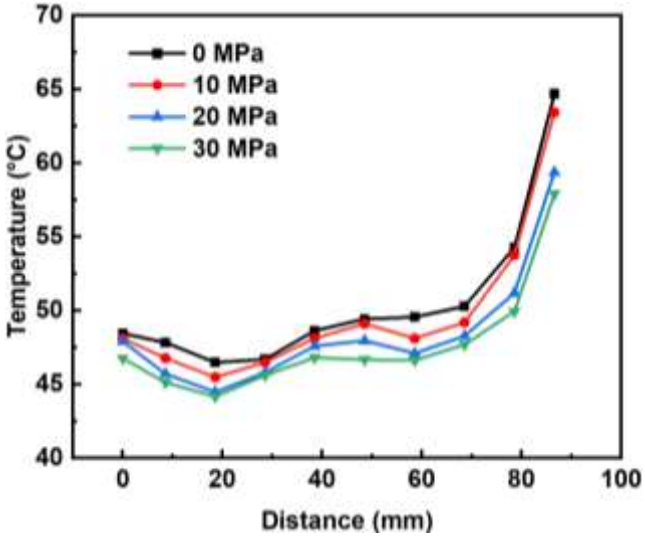

Fig. 4 Temperature along path 1 for movable auxiliary support magnitudes

3.1.2 Effect of movable auxiliary support area

As shown in Fig. 5, the temperature distribution is similar as the area of the movable auxiliary support increases, with high temperatures concentrated at the end of the workpiece. And as the area of the movable support increases, the area of the high temperature region on the machined surface decreases.

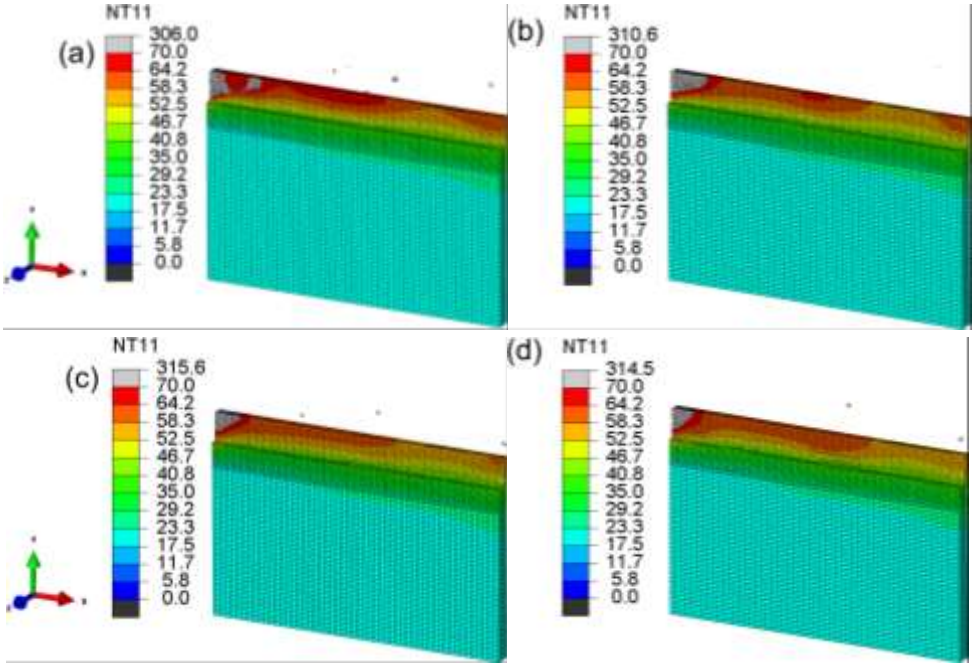

Fig. 5 Temperature distributions for movable auxiliary support areas of (a)25mm^2, (b)100 mm^2, (c)225 mm^2, (d) 400 mm^2.

Fig. 6 shows the curve of machined surface temperature under movable auxiliary support areas when the support magnitude is 20 MPa. The extraction path is also path 1. The maximum temperatures for movable auxiliary support areas of 25mm^2, 100 mm^2, 225 mm^2 and 400 mm^2 are 67.3 °C, 59.4 °C, 58.9 °C and 57.6 °C, respectively. It can be seen from the Fig.6 that as the area increases, the temperature of the machined surface decreases. This is because as the movable auxiliary support area increases, the

cutter edge becomes more streamlined in the area of contact with the workpiece, facilitating chip removal. The rapid flow of chips carries away a large amount of milling heat, accelerating heat dissipation and therefore decreasing surface temperature.

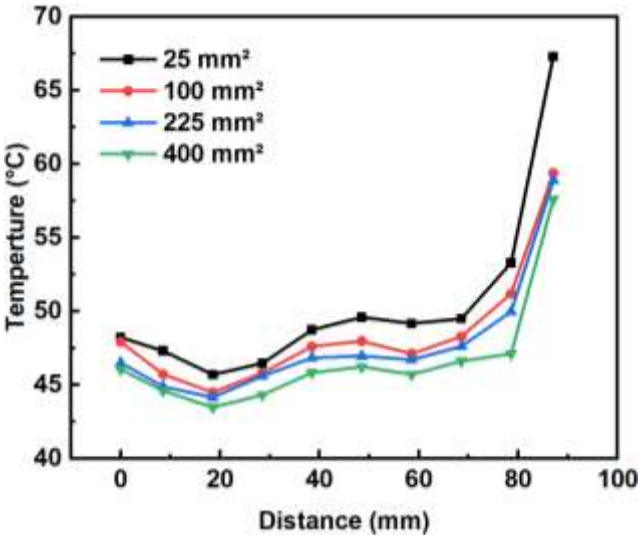

Fig. 6 Temperature along path 1 for movable auxiliary support areas

3.2 Deformation analysis

3.2.1 Effect of movable auxiliary support magnitude

Fig. 7 shows the deep direction deformation (U3) distributions of thin-walled part under movable auxiliary support magnitudes when the support is 100 mm^2. Since the change in chip displacement is also shown in the distribution graphs, and the deformation of the workpiece is relatively small, the upper and lower limits of the graphs are changed to ensure that the deformation is clearly represented. It can be seen from the figure that without the movable auxiliary support (0 MPa), the deformation of the workpiece shows a tendency to be larger at both ends and smaller in the middle. The deformation law remains essentially the same after the application of a movable auxiliary support. It is worth noting that when the movable auxiliary support increases to 30 MPa, the deformation of the middle part of the thin-walled part changes from negative to positive, when the movable auxiliary support is too large and causes the workpiece to concave towards the direction of the cutter.

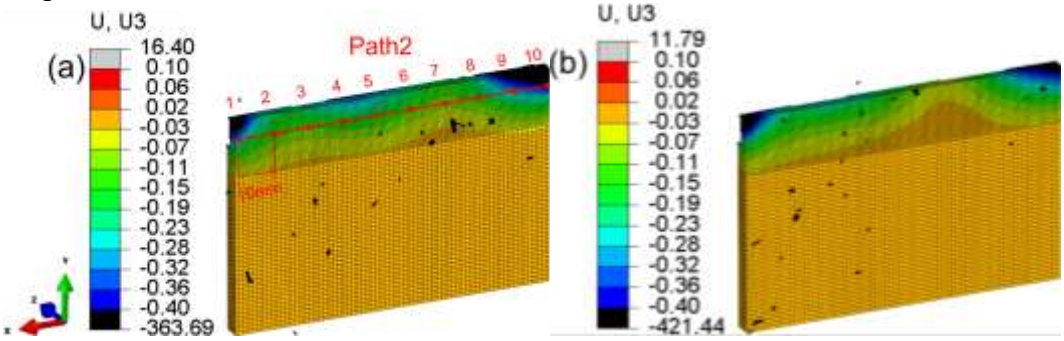

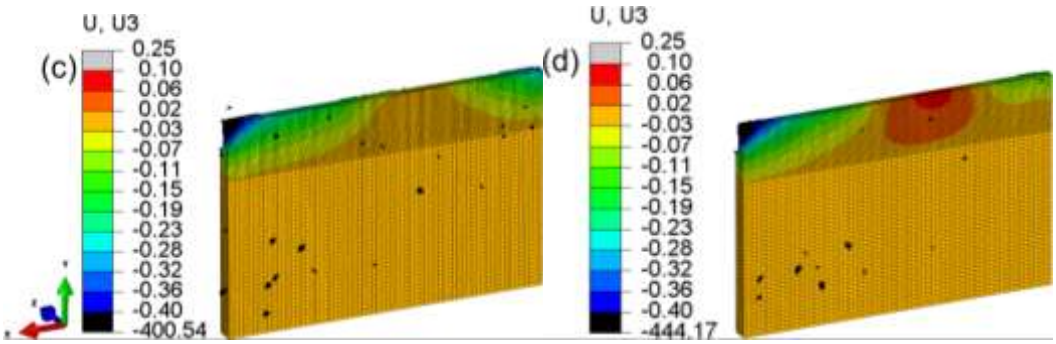

Fig. 7 Deformation distributions for movable auxiliary support magnitudes of (a) 0 MPa, (b) 10 MPa, (c), 20 MPa, (d) 30 MPa.

The back of the workpiece is an important criterion for judging the flatness of the machining, so 10 points were selected on the back of the workpiece to study the deformation law under movable auxiliary support magnitudes, each 10 mm apart, as shown in path 2 of Fig. 7a. Fig. 8 displays the curve of deformation (U3) under movable auxiliary support magnitudes when the support area is 100 mm^2. The comparison shows that in the absence of movable auxiliary support (0 MPa), the deformation of the thin-walled part is greatest at the ends and less in the middle, which is consistent with the variation in distribution graph. However, there are small fluctuations in deformation in the middle of thin-walled part, showing a tendency to increase and then decrease. After the application of the movable auxiliary support, the deformation gradually decreases as the magnitude of the movable auxiliary support increases, without a tendency to increase and then decrease in the middle part of the workpiece. The reasons for this phenomenon are as follows, in the absence of movable auxiliary support, the stiffness of thin-walled part decreases continuously as the material is removed. The stiffness of the milling area is increased with the support of the movable auxiliary support and therefore the deformation of the workpiece is reduced. It is noteworthy that the minimum deformation of the middle part of the thin-walled part is close to zero at a movable auxiliary support of 20 MPa. At a movable auxiliary support of 30 MPa, the deformation in the middle region of the thin-walled part changes from negative to positive and concaves towards the direction of the milling. At this moment the auxiliary support magnitude is too high, resulting in a change of direction of deformation in the middle region where the stiffness is low.

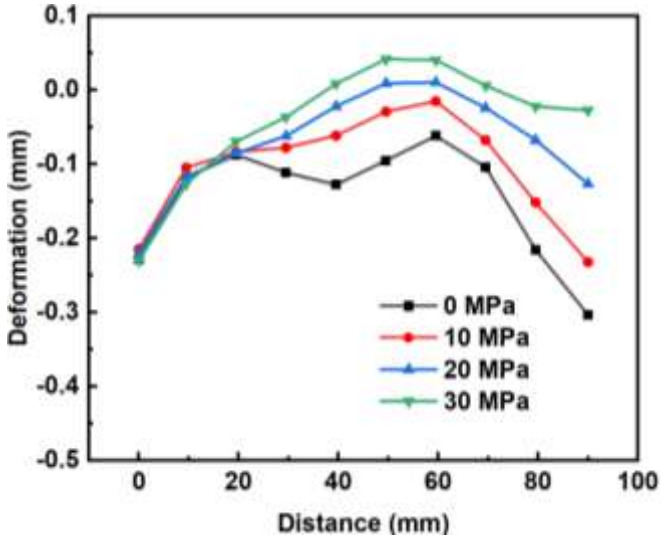

Fig. 8 Deformation along path 2 for movable auxiliary support magnitudes

3.2.2 Effect of movable auxiliary support area

Fig. 9 shows the deformation (U3) distributions of under movable auxiliary support areas when support magnitude is 20 MPa. It can be seen that the deformation of the thin-walled part gradually decreases as the movable auxiliary support area increases. When the movable auxiliary support area reaches 225 mm^2, the deformation of the middle of the thin-walled part changes from negative to positive and concaves towards the direction of the milling cutter. When the area is 400 mm^2, the deformation in the middle and end of the part turns from negative to positive and depresses in the direction of the cutter.

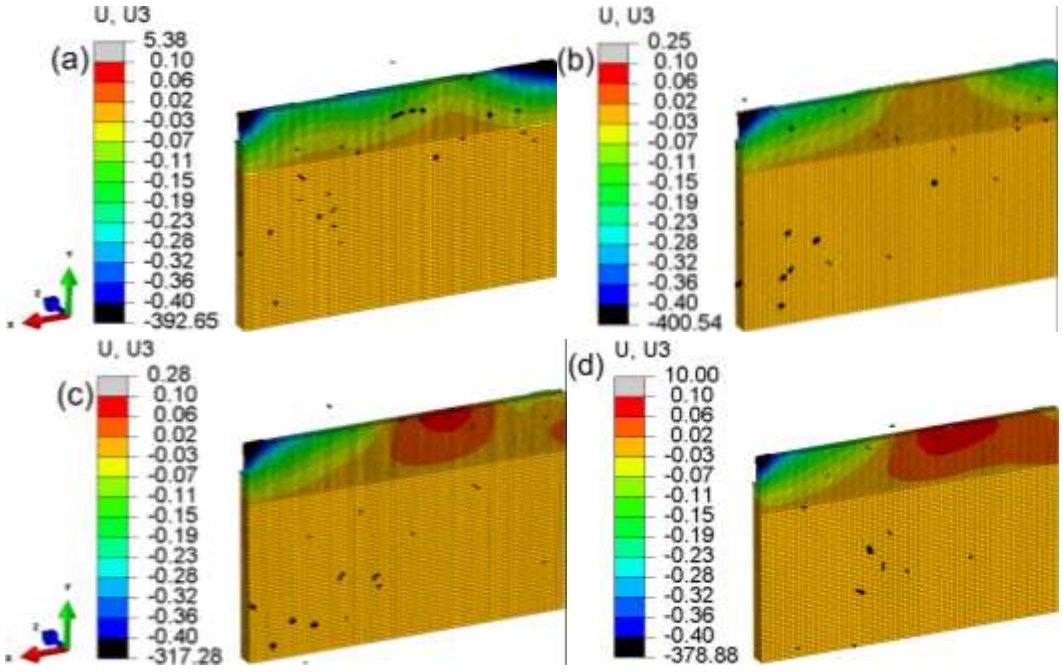

Fig.9 Deformation distributions for movable auxiliary support areas of (a)25 mm^2, (b)100 mm^2, (c)225 mm^2, (d) 400 mm^2.

Fig. 10 shows that when the movable auxiliary support is 20 MPa, the radial depth deformation (U3) of thin-walled part is extracted, and the extraction path is also path 2.

The deformation curve of the workpiece under movable auxiliary support areas can be found that, in the case of small movable auxiliary support area, the deformation at the two ends of the thin-walled part is large and the deformation in the middle is small, and there is a small increasing trend in the middle part. When a movable auxiliary support is applied, the deformation of the workpiece decreases. It is worth noting that when the movable auxiliary support exceeds 225 mm^2, both the middle part of the thin-walled part and the end of the mill change from negative to positive and depress towards the cutter.

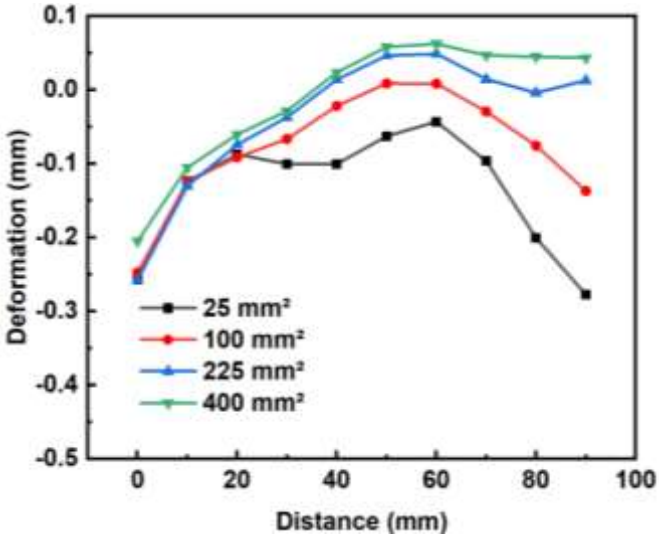

Fig. 10 Deformation along path 2 for movable auxiliary support magnitudes

3.3 Residual stress field analysis

3.3.1 Effect of movable auxiliary support magnitude

Residual stress tends to have a greater effect on thin-walled parts with low stiffness than on conventional parts. Moderate or low residual stress can also cause large secondary deformation in the part [25]. Reducing residual stress in thin-walled parts is important for improving serviceability. In general, tensile residual stress causes large secondary deformation of the thin-walled parts, whereas compressive residual stress significantly improves the fatigue life of the parts [26].

Fig. 11 shows the residual stress (S11) distributions for movable auxiliary support magnitudes. Both residual tensile and residual compressive stresses are present on the machined surface. In the absence of movable auxiliary support (0 MPA), the distribution of tensile stresses is much more extensive than that of compressive stresses. With the magnitude of the movable auxiliary support increases, the tensile residual stresses decrease and partly become compressive residual stress. And at 30 MPa, the compressive residual stresses on the machined surface have the widest distribution. The reason for this is that as the movable auxiliary support increases, the mechanical effect increases the compression of the work piece and thus creates more compressive stresses.

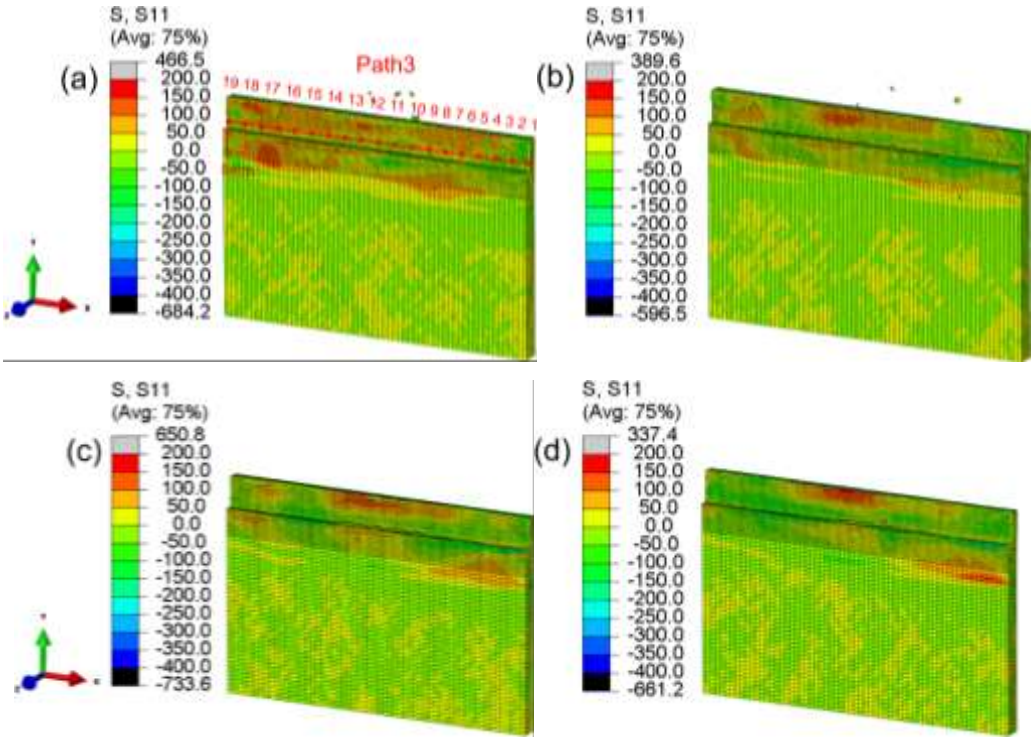

Fig. 11 Stress distributions for movable auxiliary support magnitudes of (a) 0 MPa, (b) 10 MPa, (c) 20 MPa, (d) 30 MPa.

As shown in Fig. 11a, a path with a smooth machined surface was selected to extract the residual stress (S11), with a total of 19 points, each at 5 mm intervals. Maximum residual stresses, minimum residual stresses and average residual stresses were calculated. From the Fig. 12, it can be found that the maximum residual stresses are tensile residual stresses for all four magnitudes and decrease with increasing movable auxiliary support magnitude. The average residual stresses are tensile in the absence of a movable auxiliary support, but when a movable auxiliary support is applied, the average residual stresses become compressive and increase with the movable auxiliary support magnitude. The minimum residual stresses are all compressive and increase as the movable auxiliary support increases. With the movable auxiliary support magnitude increases, this leads to an increase in mechanical stresses causing the workpiece to be squeezed and generating compressive residual stresses, which explains why tensile stresses are converted to compressive stresses. In addition, the greater the magnitude of the support, the lower the surface temperature after machining and the lower the tensile stresses generated by thermal stress. Therefore, by increasing the magnitude of the movable auxiliary support the residual tensile stress can be reduced and the compressive residual stress correspondingly increased.

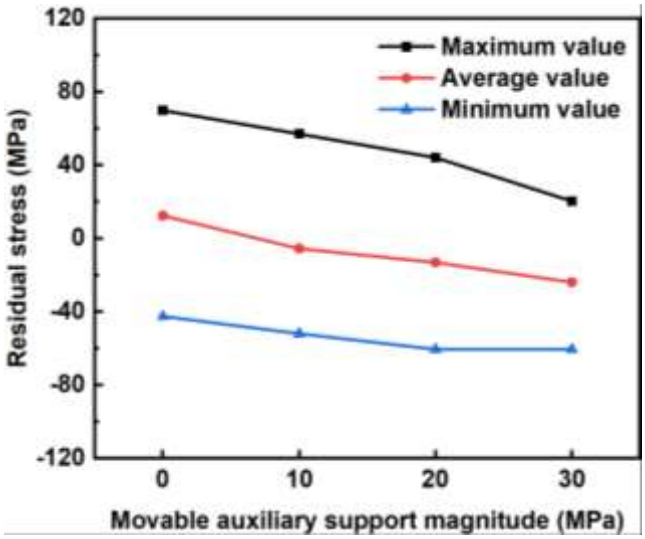

Fig. 12 Residual stress along path 3 for movable auxiliary support magnitudes

3.3.2 Effect of movable auxiliary support area

Fig. 13 shows the residual stress (S11) distributions for movable auxiliary support areas. It can be found that the distribution of residual compressive stresses on the machined surface is very small in the area of 25 mm^2. As the area of the movable auxiliary support increases, some of the tensile residual stresses decrease and become compressive residual stresses, and the range of compressive stresses increases. Between 225 mm^2 and 400 mm^2, the range of increase in compressive residual stresses is not significant, indicating that the movable auxiliary support area is best between 100 mm^2 and 225 mm^2.

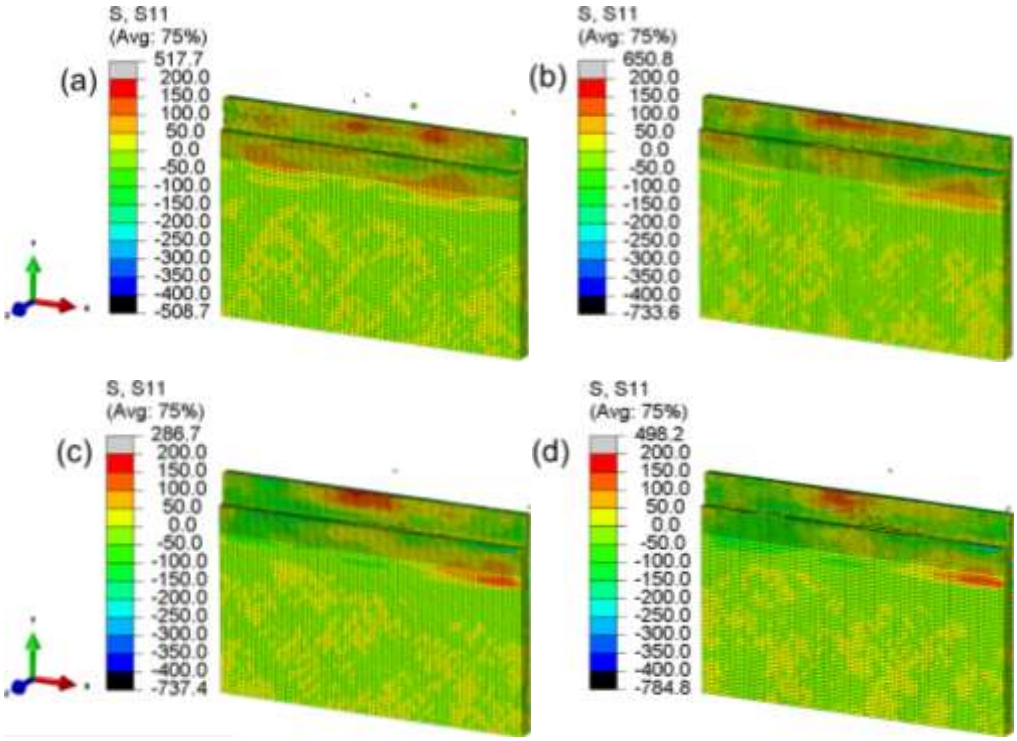

Fig. 13 Stress distributions for movable auxiliary support areas of (a)25 mm^2, (b)100 mm^2, (c)225 mm^2, (d) 400 mm^2.

Similarly, the residual stresses (S11) on the surface of the workpiece were

extracted along path 3. Maximum residual stresses, minimum residual stresses and average residual stresses were also calculated. From Fig. 14, the magnitude of the movable auxiliary support at this moment is 20 MPa and the movable auxiliary support areas are 25 mm^2, 100 mm^2, 225 $mm^2$and 400 mm^2. The maximum residual stresses are all in the form of residual tensile stresses, which tend to decrease and then increase. The average and minimum residual stresses are both compressive and show a tendency to first increase and then slowly decrease. Therefore, the effect of movable auxiliary support area on residual stress demonstrates no obvious regularity. This is probably due to the fact that the movable auxiliary support area exceeds the milling area and further increasing the support area has little effect.

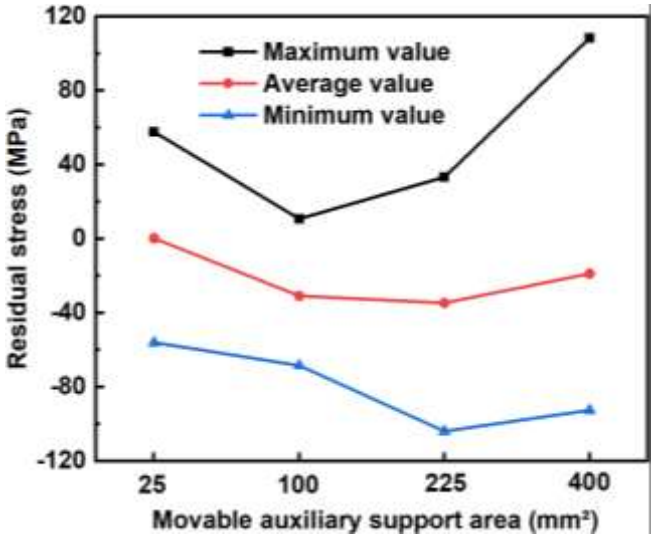

Fig. 14 Residual stress along path 3 for movable auxiliary support areas

4. Conclusions

In the present study, finite element simulation of milling 45 vol% SiCp/2024Al composites thin-walled part was carried out using thermo-mechanical coupling method, and the laws of surface temperature, deformation and residual stress were investigated for magnitudes and areas of movable auxiliary support on the backside of thin-walled part. The following conclusions can be summarized:

(1) The magnitude and area of the movable auxiliary support has a slight influence on the temperature distribution. With the increasing of magnitude and area of the movable auxiliary support, the temperature of the machined surface of thin-walled part reduces.

(2) Appropriate application of movable auxiliary support will reduce the deformation of thin-walled part, and the overall deformation of thin-walled part decreases as the movable auxiliary support magnitude and area increase. However, when the movable auxiliary support magnitude and area exceed 20 MPa or 100 mm^2, respectively, the middle of the workpiece will be concaved towards the milling cutter. Therefore, the deformation is best at a movable auxiliary support magnitude of 20 MPa and area of 100 mm^2.

(3) With the movable auxiliary support magnitude increases, the tensile residual

stresses on the surface of thin-walled part gradually decrease, changing to an increasing trend of compressive residual stresses. While the movable auxiliary support areas demonstrate no obvious regularity on the residual stress. Therefore, the compressive residual stress can be generated by increasing the auxiliary support magnitude to improve the fatigue life of the workpiece.

Authors' contributions Simulation, validation and writing were implemented by Zhijie Gao, Peng Zhu and Shu Yang. Funding acquisition, supervision and writing review were carried out by Li Zhou, Zuoshan Wei, Qitong Wang. All authors have read and agreed to published version of the manuscript.

Funding This research was supported by Ministry of Education Industry -University Cooperation Collaborative Education Project (No. BINTECH-KJZX-20220831-41).

Declarations The authors declare that they have no known competing financial interests or personal relationships that could have appeared to influence the work reported in this paper.

References

1. Gao L, Liu C, Liu JJ, Yang T (2023) Effect of subsurface damage on tensile behavior and fracture mechanism of SiCp/Al composites: Experimental analysis and RVE modeling. Eng Fail Anal 147:107162. https://doi.org/10.1016/j.engfailanal.2023.107162
2. Yu WW, Chen J, Ming WW, An QL, Chen M (2021) Experimental and FEM study of cutting mechanism and damage behavior of ceramic particles in orthogonal cutting SiCp/Al composites. Ceram Int 47: 7183-7194. https://doi.org/10.1016/j.ceramint.2020.11.072
3. Lu SJ, Wang XH, Teng LC, Zhang JJ, Zhou ZG, Tong Z, Shao HY, Men XH (2022) Finite element analysis and experimental investigation of ultrasonic testing of internal defects in SiCp/Al composites. Ceram Int 48: 5972-5982. https://doi.org/10.1016/j.ceramint.2021.11.133
4. Liu HZ, Wang SJ, Zong WJ (2019) Tool rake angle selection in micro-machining of 45 vol.% SiCp/2024Al based on its brittle-plastic properties. J Manuf Process 37: 556-562. https://doi.org/10.1016/j.jmapro.2018.12.030
5. Li BZ, Jiang XH, Yang JG, Liang SY (2015) Effects of depth of cut on the redistribution of residual stress and distortion during the milling of thin-walled part. J Mater Process Technol, 216: 223-233. https://doi.org/10.1016/j.jmatprotec.2014.09.016
6. Yue CX, Zhang JT, Liu XL, Chen ZT (2022) Advances in the study of machining deformation during the milling of thin-walled parts. AAAS, 43:524164. https://doi.org10.7527/S1000-6893.2021.25164
7. Zhang ZX, Luo M, Tang K, Zhang DH (2020) A new in-processes active control method for reducing the residual stresses induced deformation of thin-walled parts. Journal of Manufacturing Processes. J Manuf Process 59: 316-325. https://doi.org/10.1016/j.jmapro.2020.09.079
8. Wang, RQ, Xie XY, Zhou XQ, Li GF (2019) Finite element analysis of the deformation of thin-walled structural parts by milling. Modular Machine Tool & Automatic Manufacturing

Technique. https://doi.org/10.13462/j.cnki.mmtamt.2019.02.002
9. Scippa, A. Grossi N, Campatelli G, FEM based Cutting Velocity Selection for Thin Walled Part Machining. 0.0, 14: 287-292. https://doi.org/10.1016/j.procir.2014.03.023
10. Chen WS, Lv XB Duan WL (2016) Effect of tool Inclination Angle on the Elastic Deformation of Thin-walled Parts in Multi-axis Ball-end Milling. 0.0 56: 11-315. https://doi.org/10.1016/j.procir.2016.10.024
11. Zhang WY, Zhou L, Huang ST, Xu LF, Liang SW (2013) Simulation of milling deformation in thin-walled SiCp/Al composites. TE 47: 41-43. https://doi.org/10.16567/j.cnki.1000-7008.2013.10.006
12. Jia ZY, Lu XH, Gu H, Ruan FX, Liang SY (2021) Deflection prediction of micro-milling Inconel 718 thin-walled parts. Journal of Materials Processing Technology. J Mater Process Tech 291: 117003. https://doi.org/10.1016/j.jmatprotec.2020.117003
13. Fan YH, Xu YS, Hao ZP, Lin JQ (2022) Cutting deformation mechanism of SiCp/Al composites based on strain gradient theory. J Mater Process Tech 299:117345. https://doi.org/10.1016/j.jmatproter.2021.117345
14. Huang K, Yang WY (2016) Analytical modeling of residual stress formation in workpiece material due to cutting. Int J Mech Sci 114: 21-34. https://dx.doi.org/10.1016/j.ijmecsci.2016.04.018
15. Zhang PF, Zhou L, Ran YC (2019) Finite Element Analysis and Comparison of the Machinability of SiCp/Al Composite and CNT/Al Composite. Series E 101: 323-329. https://doi.org/10.1007/s40032-019-00540-y
16. Cui YZ, Gao SR, Wang FJ, Hu QM, Cheng X, Xu FX (2021) Study on the High-Speed Milling Performance of High-Volume Fraction SiCp/Al Composites. Materials 14: 4143. https://doi.org/10.3390/mal4154143
17. Wu Q, Xie DJ, Si Y, Zhang YD, Li L, Zhao YX (2018) Simulation analysis and experimental study of milling surface residual stress of Ti-10V-2Fe-3Al. J Manuf Process 32: 530-537. https://doi.org/10.1016/j.jmapro.2018.03.015
18. Kong XJ, Ding ZS, Xu LJ, Zhu LJ, Zhang J, Wu CJ, Isaev A (2019) Effects of Milling Parameters on Distribution of Residual Stress During the Milling of Curved Thin-Walled Parts. EPJ Web Confer 224: 05009. https://doi.org/10.1051/epjconf/201922405009
19. Wang ZJ, Chen WY, Zhang YD, Chen ZT, Liu Q (2005) Study on the Machining Distortion of Thin-walled Part Caused by Redistribution of Residual Stress. Chinese J Aeronaut 18: 175-179. https://doi.org/10.1016/S1000-9361(11)60325-7
20. Wu Q, Li DP, Zhang YD (2016) Detecting Milling Deformation in 7075 Aluminum Alloy Aeronautical Monolithic Components Using the Quasi-Symmetric Machining Method. Metals 6. https://doi.org/10.3390/met6040080
21. Wang T, Xie LJ, Wang XB (2015) Simulation study on defect formation mechanism of the machined surface in milling of high-volume fraction SiCp/Al composite. Int. J. Adv. Manuf. Technol 79:1185-1194. https://dio.org/10.1007/s00170-015-6876-x
22. Wang X (2019) Aluminum-based silicon carbide micromachining simulation method and surface integrity study. CUST.
23. Zhou L, Cui C, Zhang PF, Ma ZY (2016) Finite element and experimental analysis of machinability during machining of high-volume fraction SiCp/Al composites. Int. J. Adv. Manuf. Technol 91: 1935-1944. https://dio.org/10.1007/s00170-016-9933-1

24. Chen G, Gao Q, Yang XP, Liu J, Su YX, Ren CZ (2022) Investigation of heat partition and instantaneous temperature in milling of Ti-6Al-4V alloy. J Manuf Process 80:302-319. https://doi,org/10.1016/j.jmapro.2022.05.051
25. Jiang XH, Kong XJ, He SR, Wu K (2021) Modeling the superposition of residual stresses induced by cutting force and heat during the milling of thin-walled parts. J Manuf Process 68: 356-370. https://doi.org/10.1016/j.jmapro.2021.05.048
26. Tan L, Zhang DH, Yao CF, Wu DX, Zhang JY (2017) Evolution and empirical modeling of compressive residual stress profile after milling, polishing and shot peening for TC17 alloy. J Manuf Process 26: 155-165. https://dx.doi.org/10.1016/j.jmapro.2017.02.002